# Non-self-similar viscous gravity currents

Bruce R. Sutherland,[1,2,*] Kristen Cote,[1,†] Youn Sub (Dominic) Hong,[3]
Luke Steverango,[4] and Chris Surma[5]

[1]*Department of Physics, University of Alberta, Edmonton, Alberta, T6G 2E1, Canada*
[2]*Department of Earth and Atmospheric Sciences, University of Alberta, Edmonton, Alberta, T6G 2E3, Canada*
[3]*Department of Engineering Science, University of Toronto, Toronto, Ontario, M5S 1A1, Canada*
[4]*Department of Mathematics, McGill University, Montreal, Quebec, Canada*
[5]*Department of Mechanical Engineering, University of Alberta, Edmonton, Alberta, Canada*

(Received 2 November 2017; published 15 March 2018)

Lock-release experiments are performed focusing upon the evolution of near-pure glycerol flowing into fresh water. If the lock height is sufficiently tall, the current is found to propagate for many lock lengths close to the speed predicted for energy-conserving moderately non-Boussinesq gravity currents. The current then slows to a near stop as the current head ceases to be elevated relative to its tail and the current as a whole forms a wedge shape. By contrast, an experiment of near-pure glycerol advancing under air exhibits the well-known slowing of the current such that the front position increases as a one-fifth power of time. The evolution of a viscous gravity current in water is also qualitatively different from that for a high-Reynolds number gravity current which transitions smoothly from a constant speed to self-similar to viscous regime. The reason a viscous gravity current flowing under water moves initially at near-constant speed is not due to a lubrication layer forming below the current. Rather it is due to the return flow of water into the lock establishing a current with an elevated head that is taller than the viscous boundary layer depth near the current nose. The flow near the top of the head advances to the nose where it comes into contact with the tank bottom. Meanwhile the ambient fluid is pushed up and over the head rather than being drawn underneath it. The front slows rapidly to a near stop as the head height reduces to that comparable to the boundary layer depth underneath the head. The initial speed and entrainment into the current are shown to depend upon the ratio, $R_\ell$, of the starting current height to the characteristic boundary layer depth. In particular, entrainment via the turbulent shear flow over the head is found to increase the volume by less than 10% during its evolution if $R_\ell \lesssim 10$ but increases by as much as 100% for high-Reynolds number gravity currents. A conceptual model is developed that captures the transition from an inertially driven current to its sudden near stop by viscous forces.

DOI: 10.1103/PhysRevFluids.3.034101

## I. INTRODUCTION

Gravity currents, also called density currents, move horizontally due to the difference in density between the current and the surrounding ambient fluid. Such is the case for example of sea breezes, dust storms, and the accidental sudden release of heavy gas [1,2]. In the laboratory a standard method for producing gravity currents is through lock-release experiments in which dense fluid behind a gate

*bruce.sutherland@ualberta.ca; https://www.ualberta.ca/~bsuther
†Present address: Department of Earth and Space Science and Engineering, York University, Toronto, Ontario, Canada.

 

is suddenly released into the ambient fluid on the other side by rapid vertical extraction of the gate. In sufficiently long tanks with relatively short locks the typical evolution of the current passes through three stages: the slumping (or steady-state) regime in which the current nose propagates at constant speed, the self-similar regime in which the front slows as a consequence of the finite-length lock, and the viscous regime in which the tangential stress of the tank bottom acting on the fluid significantly slows the front [3–6]. Of course, if the fluid in the lock is very viscous, one would expect after release that the current should rapidly enter the viscous regime. This circumstance was examined by Huppert [5], who derived a differential equation determining the height of the current along its length as it advanced in time. Assuming the shape was self-similar, he found an explicit analytic expression for the current height and nose position. His predictions were found to be consistent with experiments he performed of silicone oil released from a cylinder and spreading axisymmetrically into air.

Motivating the study presented here, we asked how the evolution of a viscous gravity current would be affected if it could mix with a significantly less viscous ambient fluid. Such mixing, where it occurs, would reduce the current's viscosity and so render it susceptible to more mixing. However, in performing laboratory experiments of glycerol moving into water it was found that, even with apparently negligible mixing, the current evolved qualitatively differently than would a current of glycerol moving into air. The current front is found to move at near constant speed for many lock lengths and then rapidly slows to a near stop. The self-similar power-law behavior associated with the front position versus time in the buoyancy-inertia regime is not evident.

In Sec. II we review the relevant aspects of the theory for steady inviscid gravity currents and for viscous gravity currents. After describing the experiment setup in Sec. III, we present the qualitative and quantitative results for viscous gravity currents in air and water. In Sec. IV we combine the results of many experiments to form scaling-based predictions of the speed, near-stopping distance, and entrainment as they depend upon the initial current height relative to a characteristic boundary layer depth. Based upon these results a conceptual model is developed in Sec. V for Boussinesq viscous gravity currents released from relatively tall locks. This is shown to capture the key features of the experiments. The results are discussed in Sec. VI.

## II. GRAVITY CURRENT THEORY

The steady propagation speed of inviscid gravity currents was considered first by von Kármán [7] and then more generally in a seminal paper by Benjamin [3] who used mass and momentum conservation in a control volume surrounding the current head in a reference frame moving with the head. In particular, assuming no loss of energy in the ambient fluid flowing toward and over the current head, and assuming the dense fluid in the lock has the same depth as the ambient fluid (a "full-depth lock-release" experiment), the current is predicted to propagate at speed

$$U_H = \sqrt{g'H}/2, \tag{1}$$

in which $H$ is the height of the ambient fluid. Because the near-pure glycerol used in our experiments is 26% denser than fresh water, we define the reduced gravity by $g' = g(\rho_\ell - \rho_0)/\rho_\ell$, which is appropriate for Boussinesq and moderately non-Boussinesq gravity currents [8,9]. In this expression, $\rho_\ell$ is the current density and $\rho_0$ is the ambient fluid density. The height, $h$, of this energy-conserving current well behind the head is predicted to be half that of the domain: $h = H/2$. Thus, in terms of the current height, the speed is

$$U_h = \frac{1}{\sqrt{2}}\sqrt{g'h}. \tag{2}$$

In studies of partial-depth lock-release currents, Shin *et al.* [10] predicted the current height, $h$, should be half that of the depth of the lock fluid and the speed of the front should be

$$U_h = \sqrt{g'h}\sqrt{1 - h/H}. \tag{3}$$

This differs from the empirical expression found by Huppert and Simpson [11]. But it was found, within error, to predict the speeds observed in their laboratory experiments. It was suggested that the discrepancy with the empirical relation was due in part to the challenge in accurately measuring $h$ in a flow that in fact exhibits mixing over and behind the head due to the turbulent shear at the interface between the miscible liquids.

Crucial to the predictions of the current speed is the influence of the return flow over the head whose inertia due to Bernoulli's principle establishes an adverse horizontal pressure gradient [3,12]. The speed of the return flow over and behind the head is faster if the relative current depth $h/H$ is larger and so the magnitude of the horizontal pressure gradient over the current increases, slowing the speed that the current would have if the ambient fluid was effectively infinitely deep. In particular, for a gravity current in air Huppert and Simpson [11] empirically determined the ratio $U_h/\sqrt{gh}$ to be 1.19 whereas von Kármán [7] used shallow water theory to predict a ratio of $\sqrt{2}$.

If the lock fluid is significantly more viscous than the ambient fluid, then continuity of the shear stress at the interface between these fluids suggests the vertical shear near the top of the current is approximately zero [5]. The advance of the current nonetheless is retarded by the action of viscous stresses resulting from the motion of the current over a rigid bottom boundary. In the limit of a shallow-water flow in which the viscous boundary layer is assumed to extend through the depth of the current, the velocity within the current is set entirely by a balance between viscous stresses and the horizontal pressure gradient, which itself is set by hydrostatic balance. Requiring no-slip flow at the bottom, where $z = 0$, and no stress at the top, where $z = h$, the velocity is found to be [5]

$$u = -\frac{1}{2}\frac{g'}{\nu}\frac{\partial h}{\partial x} z(2h - z), \tag{4}$$

in which $\nu$ is the kinematic viscosity of the current.

The time evolution of the viscous current is given by the condition for mass conservation [5]:

$$\frac{\partial h}{\partial t} = -\frac{\partial}{\partial x}\left[\int_0^h u\, dz\right] = \frac{1}{3}\frac{g'}{\nu}\frac{\partial}{\partial x}\left[h^3\frac{\partial h}{\partial x}\right]. \tag{5}$$

In particular, for a viscous current produced by release from a lock of height $H_\ell$ and length $L_\ell$, a self-similar solution can be found for (5) such that [5]

$$h(x,t) \propto t^{-1/5}\phi(\beta x t^{-1/5}) \tag{6}$$

in which $\beta$ is a constant depending on $g'$, $\nu$ and the product of the lock height and length, $H_\ell L_\ell$. The shape function is

$$\phi(\tilde{x}) \propto (1 - \tilde{x}^2)^{1/3}. \tag{7}$$

Thus the current nose [situated where $h(\tilde{x} = 1) = 0$] is expected to advance in time as $x_N \propto t^{1/5}$.

We now turn to the examination of the experiments presented herein. We consider a fluid of kinematic viscosity $\nu$ much larger than the viscosity, $\nu_0$ of the ambient fluid. But we suppose that its density, $\rho_\ell$, is only moderately larger than the ambient fluid density, $\rho_0$. In particular, for our experiments of near-pure glycerol moving into water, the viscosity ratio is $\nu_0/\nu \simeq 0.001$ whereas the density ratio is $\gamma = \rho_0/\rho_\ell \simeq 0.79$. It is also assumed that the diffusivity, $\kappa$, of the viscous fluid is much smaller than its kinematic viscosity (for glycerol in water, the Schmidt number is $\mathrm{Sc} \equiv \nu/\kappa \simeq 1.1 \times 10^3$). So diffusion has negligible influence upon the evolution of the currents [13].

After extraction of the gate, the horizontal density gradient between the lock fluid and ambient fluid acts to accelerate the fluid leaving the lock. Two opposing forces act upon this fluid. One comes from tangential stresses exerted from the bottom and sides of the tank. Of these, the bottom stress is ultimately expected to be most significant: as the current advances and its height decreases, the vertical scale of the current becomes the smallest in the system. However, even this stress takes time to exert itself through the depth of the current. A simple scaling predicts that after the current nose has passed a fixed location the viscous boundary layer above that point should grow at a rate

given by

$$\delta \sim \sqrt{\nu t_N}, \tag{8}$$

in which $t_N$ measures the time since the nose passed over that location. If $\delta$ is much less than the current height at the position, then viscosity should not act significantly to retard the advance of the current nose.

The second force comes from the return flow passing over the advancing current and flowing toward and into the lock. Because $\nu \gg \nu_0$ and $\rho \gtrsim \rho_0$, the balance of tangential stresses in the current and ambient fluid acting at the interface between them suggests the vertical shear in the current near the interface is negligibly small [5]. Thus viscous stresses are likewise negligible. However, the return flow establishes an adverse pressure gradient along the interface between the current and ambient fluid. This reduces the total horizontal pressure gradient within the current from that given by hydrostatic balance alone. Neglecting energy dissipation in the return flow as well as viscous forces at the bottom and side boundaries, the anticipated current speed is expected to be that for an inviscid gravity current. That is, for $\delta \ll z \leqslant h$, the fluid within the advancing current front is expected to move at speed $U_h$ given by (3) in which $h = H_\ell/2$.

Away from the viscous boundary layers, the motion of viscous fluid in the lock is expected to correspond approximately to that of potential flow such that

$$(U_\ell, W_\ell) \simeq \left( U_h \frac{x-\delta}{L_\ell}, -U_h \frac{z-\delta}{L_\ell} \right). \tag{9}$$

As the current nose advances from the lock, the viscous boundary layer trailing the nose grows until $\delta$ becomes comparable to $h$ in which case the flow slows over the whole vertical extent of the current. However, the boundary layer depth is infinitesimally small at the nose itself. And so the nose is expected to advance at speed close to $U_h$ until the head is depleted of fluid due to viscosity slowing the fluid behind the head.

Based upon these arguments, an estimate of how high the lock fluid must be in order for the current it generates to advance at speed $U_h$ is given by a comparison of the current height $H_\ell/2$ to the characteristic boundary layer height, $\delta_\ell$, after the current has propagated one lock length at constant speed $U_h$. Using (8), we set $\delta_\ell \sim \sqrt{\nu L_\ell / U_h}$. Explicitly the ratio is given by the nondimensional parameter

$$R_\ell = \sqrt{\alpha \mathrm{Re}/2}, \qquad \text{with } \alpha \equiv H_\ell/L_\ell, \quad \mathrm{Re} \equiv U_h(H_\ell/2)/\nu. \tag{10}$$

Here $\alpha$ is the aspect ratio of the lock fluid and Re is the Reynolds number based upon the initial current height. We refer to the gravity current as being "moderately viscous" if $R_\ell$ is of order unity.

## III. EXPERIMENT SETUP AND QUALITATIVE RESULTS

Here we describe the setup of the experiments and the analysis techniques used to measure the front position and the current height as they evolve in time. From the latter we assess entrainment by changes to the vertical-streamwise cross-sectional area (the volume per unit width) of the current over time. The evolution of currents composed of near-pure glycerol moving into water are compared with classic experiments of glycerol moving into air and of salt water moving into water.

Figure 1 shows a snapshot of an experiment just before it begins. Experiments were performed in a rectangular glass tank with internal dimensions of length $L_T = 197.1$ cm, width $W_T = 17.5$ cm, and height $H_T = 48.6$ cm. The side walls and bottom were 1.2 cm thick. The tank was backlit either with a bank of four horizontally stacked 2-m-long fluorescent bulbs or with two white LED spot lamps. In either case the light was diffused through two layers of translucent white acrylic sheets placed against the back wall of the tank. In many experiments a 124-cm-long mirror angled at 36.4° from the horizontal was situated above the tank midway along its length thus providing simultaneous top and side views of an experiment with respect to a camera situated approximately 3 m in front of the tank and with a lens at the level of the bottom of the tank. For these experiments, the tank

FIG. 1. Snapshot from an experiment just before gate is extracted. For this experiment the dyed lock fluid is 99.2% glycerol situated in a lock of width $\ell = 8.3$ cm. The ambient fluid to the right of the gate is fresh water (the superimposed dashed line indicates its surface). The height of both lock and ambient fluids is 19.9 cm. The angled mirror above the tank gives top views of the ensuing flow between approximately 50 and 130 cm from the left end of the tank.

was bottom-supported by benches on the left and right ends of the tank, while the middle section was illuminated from below by a fluorescent light shining on matt-finish Mylar film taped to the underside of the tank.

A gate was inserted in one of the five pairs of 0.1-cm-thick vertical glass guides. Foam tape around the edges of the gate ensured a good seal with the tank side walls and bottom so that fluid would not pass around or below the gate between the lock and ambient fluid. A viscous liquid of density $\rho_\ell$ and viscosity $\nu_\ell$ was added to the lock to a predetermined depth, $H_\ell$. In some experiments up to 20 drops of food colouring were added to the lock fluid in order to distinguish it from the clear ambient fluid. In most cases the lock fluid was near-pure or diluted glycerol. Its density was measured to five-digit accuracy with a densitometer (Anton Paar, DMA4500). From the density measurement, the viscosity was estimated by a cubic spline interpolation of values of viscosity versus density of glycerol as tabulated in Ref. [14]. The viscosity of glycerol decreases significantly as it becomes diluted, dropping by nearly half of its pure value if its concentration is 96%. While this is disadvantageous for many studies of viscous flows, we use glycerol here in part to examine the positive feedback whereby possible mixing around the current head may reduce its viscosity thus further enhancing mixing.

After the glycerol was added to the lock, time was given for any bubbles entrained into the glycerol during the filling process to rise to the surface (up to an hour for near-pure glycerol). Meanwhile, ambient fluid of density $\rho_0 < \rho_\ell$ and viscosity $\nu_0 \ll \nu_\ell$ (typically fresh water) was added to the right of the gate. In full-depth lock-release experiments, the ambient fluid was added to the height, $H = H_\ell$, of the lock fluid. In partial-depth lock-release experiments, the ambient was filled to depth $H > H_\ell$ and ambient fluid was slowly added above the glycerol to a total lock height moderately smaller than $H$, set so that the hydrostatic pressure at the bottom was the same on either side of the gate (accounting for the fact, for example, that pure glycerol is about 26% more dense than fresh water).

Movies of the experiment were taken with a digital camera (Canon Rebel T3i) at a resolution of 1980 by 1080 pixels per frame and recorded at 29.97 frames per second. These were cropped and converted in MPEG movies at 24 frames per second that were then processed using MATLAB to extract snapshots, create horizontal time series, and perform analyses to find the current height along its length at each time during the current's evolution. The typical pixel resolution was 0.1 cm/pixel in the horizontal and vertical. However, the actual resolution is closer to twice this value due to filtering in the camera and conversion to MPEG format.

As an example of these analysis methods, Fig. 2 shows side-view snapshots of the classic experiment in which a rectilinear viscous gravity current collapses into air. After rapidly advancing from the lock in the first second its progress slows significantly. At all times the current height increases monotonically from the nose to the lock end of the tank. Indeed, the current height along its full length is well predicted by the formula for a self-similar gravity current according to (7). The dotted curve in the bottom image of Fig. 2 is the plot of $h(x) = h_0[1 - (x/\mathrm{x_N})^2]^{1/3}$ with $h_0 = 3.2$ cm and $\mathrm{x_N} = 82$ cm.

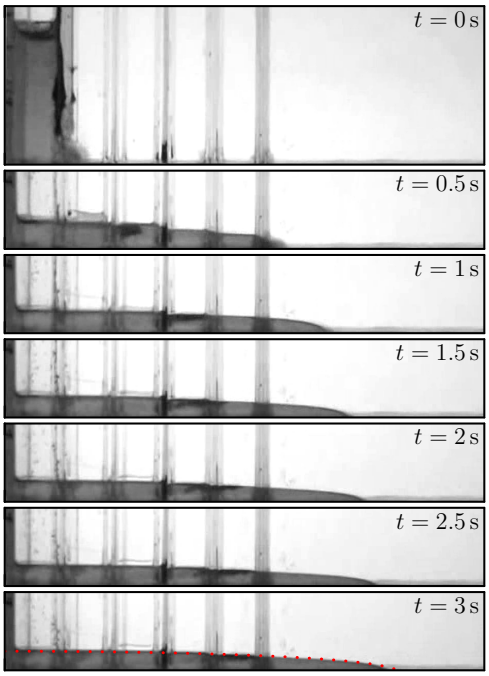


FIG. 2. Snapshots taken from an experiment with 99.2% glycerol collapsing into air [17]. Initial conditions are $H_\ell = 19.9\,\mathrm{cm}$, $L_\ell = 8.3\,\mathrm{cm}$, $\rho_\ell = 1.2590\ \mathrm{g/cm^3}$, and $\nu_\ell = 10.40\ \mathrm{cm^2/s}$. Only the leftmost 97 cm of the tank is shown, and all but the top image shows the bottom 9 cm. The times of each snapshot are indicated at the upper right of each frame. The dotted red line superimposed on the bottom image plots the shape predicted for a self-similar viscous current given by (7).

The corresponding horizontal time series is constructed by taking horizontal slices through successive snapshots at a pixel location corresponding to 0.1 cm above the bottom of the tank. The result is shown in Fig. 3(a). The regular horizontal banding in this image is due to a strobing effect between the frequency of the lighting and the camera frame rate. Using image-processing techniques, these horizontal bands and the vertical features (due to the glass guides for each lock and other irregular marks near the tank bottom) can be filtered out so that the distance of the gravity current nose from the gate can be tracked in time. This curve, denoted by $x_N(t)$, is indicated by the white dashed line in Fig. 3(a) and is graphed as a log-log plot of position versus time in Fig. 3(b). The jagged features of this curve at times before 0.5 s are a consequence of the pixel and time resolution. Such resolution limitations are not an issue after 0.5 s. In particular, it is clear that a few seconds after release the front advances according the predicted power law $x_N \propto t^{1/5}$.

That the shape of the current and its advance agree well with the theory for one-dimensional (spanwise infinite) viscous gravity currents provides good evidence that viscous stresses at the side walls of the tank do not play a significant role in affecting the front's advance.

In comparison, we show snapshots and time series for an experiment of 99.2% glycerol collapsing into fresh water, the initial setup for which is shown in Fig. 1. The reduced gravity of the current is $g' = g(\rho_\ell - \rho_0)/\rho_\ell \simeq 0.21g$, in which $g$ is gravity. Hence the speed of the current is expected to be about 45% that of the corresponding gravity current collapsing into air. For this reason, the snapshots in Fig. 4 are shown every second, whereas those for the gravity current in air are shown every half second in Fig. 2. These snapshots clearly show that the evolution of the current is qualitatively different. Whereas the height of the gravity current in air monotonically increases from nose to tail for all times, shortly after release the gravity current moving into water develops a clearly defined elevated head such that the current height reaches a maximum moderately behind the nose. The

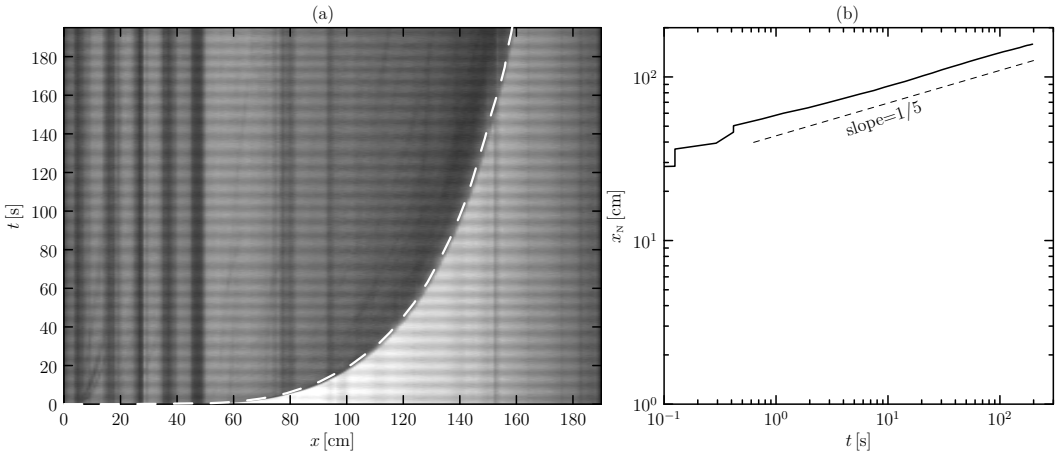


FIG. 3. (a) Horizontal time series constructed from successive horizontal slices taken 0.1 cm above the bottom of the tank for the experiment with snapshots shown in Fig. 2. The superimposed white dashed line indicates the measured front position. (b) Log-log plot of corresponding front position versus time. The offset dashed line with one-fifth slope is that predicted for viscous gravity currents [4,5]. Note that the horizontal banding in (a) is due to a stroboscopic effect between the camera's frame rate and the 60 Hz background lighting used in this experiment.

current height decreases behind the head and then increases again, albeit slowly, along the tail to the lock end of the tank. The elevated head persists though its height and length decrease as the gravity current propagates along the bottom until time $t \gtrsim 6$ s when the head flattens and the current as a whole adopts the approximate shape of a wedge. Although this shape monotonically increases from the nose to the tail, its structure is not that given by the formula (7) for self-similar viscous gravity currents. For example, superimposed on the bottom image is the height predicted for a self-similar gravity current using $h_0 = 2.4$ cm for the depth at the lock end of the tank and $x_N = 125$ cm for the nose position. The height of the actual current is well below this curve over three fourths of its length behind the nose. This suggests that near the current's front viscous forces dominate over buoyancy forces manifest through horizontal pressure gradient forces set by hydrostatic balance.

The corresponding top-view snapshots in Fig. 5 show that the front is nearly uniform across the span of the tank with some evidence of the viscous no-slip condition of the side walls extending about a half-centimeter inwards from each wall. There is no evidence of lobe-and-cleft instabilities developing along the front as has been observed for high Reynolds number gravity currents [15].

The horizontal time series is constructed from snapshots of this experiment by taking slices 0.1 cm above the bottom of the tank. This reveals that the advance of the front position is also qualitatively different from that of a gravity current moving into air. As shown in Fig. 6, the front advances as far as 60 cm (seven lock lengths) from the gate with little deceleration. Indeed, even though the initial current speed is less than half that of the corresponding gravity current in air, comparison of Fig. 4 and Fig. 2 at $t = 3$ s shows that the nose of the gravity current in water is close to the position of the nose of the gravity current in air. Although the speed of the latter is initially much faster, it rapidly slows down, whereas the current in water advances at near-constant speed.

Also different from a gravity current in air, the advance of the front does not enter into the regime where $x_N \propto t^{1/5}$, as predicted for a self-similar current in the viscous-buoyancy regime. Instead the speed of the current rapidly decelerates almost to zero around $t = 7$ s. It is at this time that the elevated head of the current has flattened out and, as argued above, viscous forces near the current front dominate over buoyancy forces. Although it appears to stop, the nose nonetheless advances slowly: it travels the remaining 80 cm to the end of the tank over tens of minutes while the current height gradually flattens out along its length.

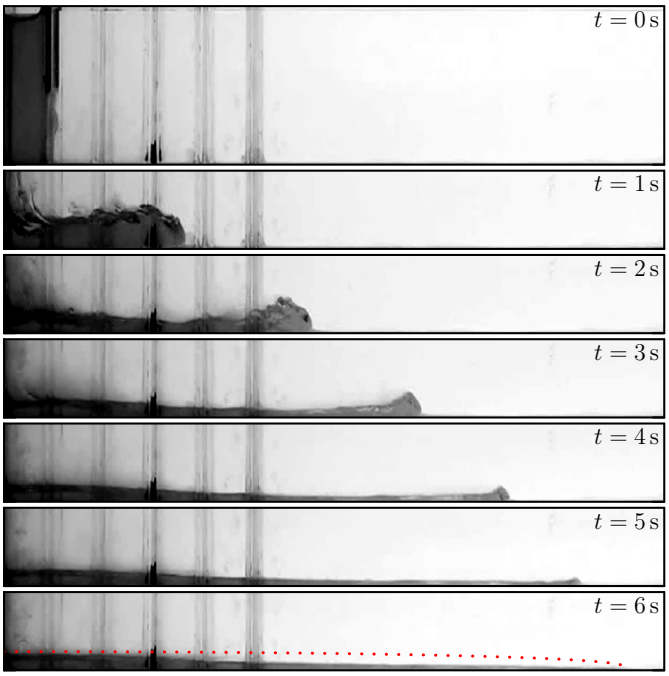


FIG. 4. As in Fig. 2 but showing snapshots taken from an experiment of near-pure glycerol collapsing into water having initial condition shown in Fig. 1 [17]. The time $t = 0$ is taken to be when the gate has been lifted halfway out of the lock and just before the viscous fluid begins to slump out of the gate. Only the leftmost 130 cm of the tank is shown, and all but the top image show the bottom 10 cm. The dotted red line superimposed on the bottom image plots the shape predicted for a self-similar viscous current given by (7).

Entrainment into the gravity current was examined in one set of experiments by allowing potassium permanganate crystals to settle and partially dissolve on the bottom of the tank in the ambient fluid of fresh water several lock lengths ahead of the gate. Of the two experiments shown in Fig. 7, the left column of snapshots shows the advance of a salt-water gravity current ($\rho_\ell = 1.14\ \mathrm{g/cm^3}$, $\nu_\ell = 0.014\ \mathrm{cm^2/s}$) whereas the right column shows the advance of a nearly pure

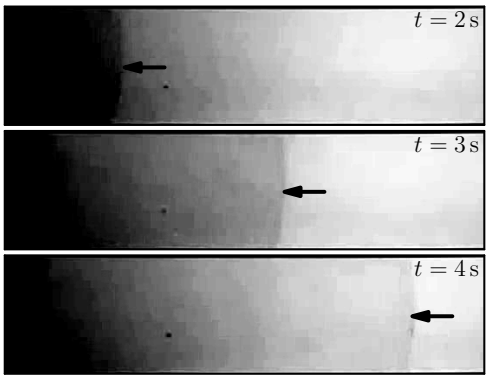


FIG. 5. Top views of the experiment with side-views shown in Fig. 4 as seen at $t = 2$, 3, and 4 s from the angled mirror above the tank between 50 cm and 140 cm from the lock end of the tank. Superimposed black arrows point to the location of the front at midspan in the tank.

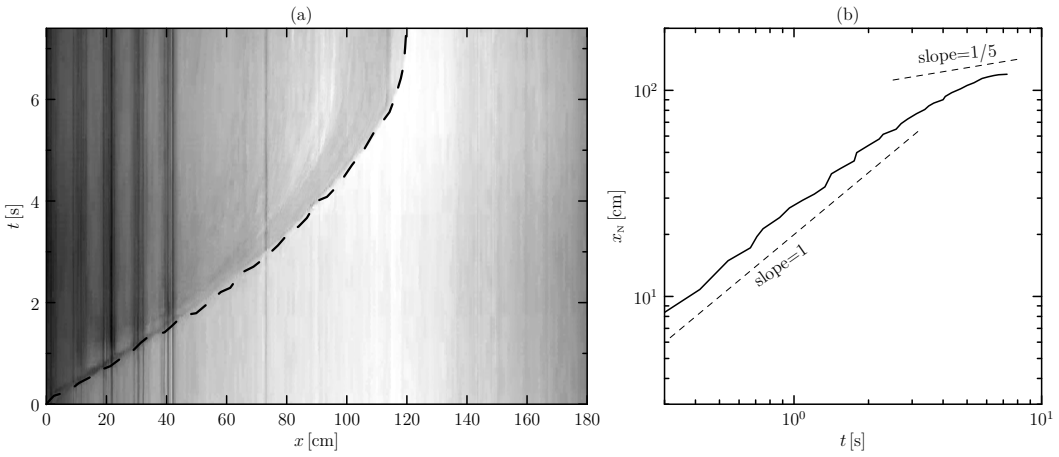


FIG. 6. (a) Horizontal time series and (b) front position as in Fig. 3 but shown for a gravity current moving into water, with corresponding snapshots shown in Fig, 4. The dashed line with one-fifth slope is drawn to indicate that the front does not enter the classical viscous regime for any appreciable time.

glycerol gravity current ($\rho_\ell = 1.26$ g/cm$^3$, $\nu_\ell = 10.6$ cm$^2$/s). The dye is carried into the salt-water current from below whereas for the glycerol current the dye is swept up and over the current without entraining into the head. A top view (not shown) of the glycerol experiments reveals that the crystals themselves move little from their original positions at the bottom of the tank. These observations suggest that there is no lubrication layer of fresh water that is drawn under the viscous gravity current. Rather, as in the case of a viscous gravity current in air, the head rolls out like an unfurling carpet with flow near the top of the head advancing to the nose where it comes into contact with the bottom.

From side-view snapshots of the current at successive times, using MATLAB we track the interface between the current and ambient fluid by setting an intensity threshold to be the ambient fluid intensity less 10% of the intensity difference between that of the ambient fluid and of the current well below the interface. Thus at each time we measure the current height $h(x,t)$. The algorithm fails at early times within the lock region due to viscous fluid running down the side walls of the tank after the

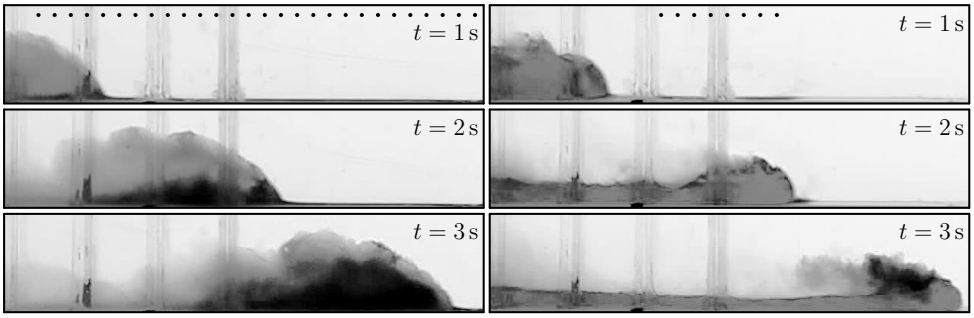


FIG. 7. Snapshots at times $t = 1, 2, 3$ s from experiments with salt water advancing into water (left column) and nearly pure glycerol advancing into water (right column) [17]. Each frame shows a window extending between 20 and 90 cm from the lock end of the tank and extending 10 cm from the bottom in full-depth lock-release experiments with total depth 20 cm. Potassium permanganate crystals are placed along the bottom of the tank over the range indicated by the dotted lines in the top two panels. The experiments compare how dye from the partially dissolved crystals is carried by the currents in each circumstance. In all images the intensity has been adjusted to enhance the contrast between the current (medium gray) and potassium permanganate (black).

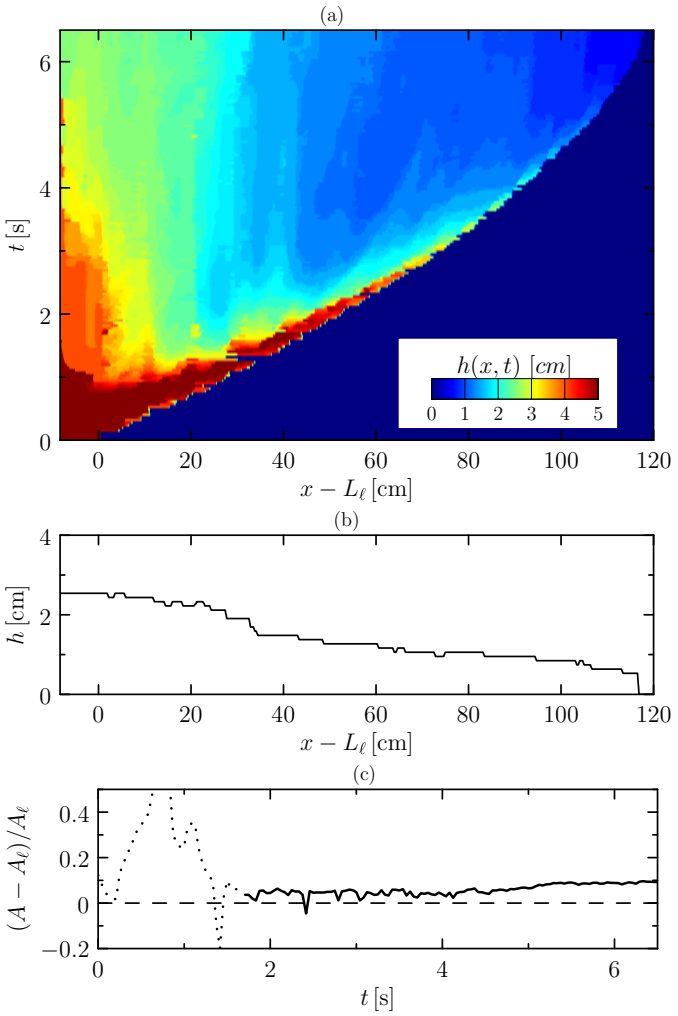


FIG. 8. For the experiment with snapshots shown in Fig. 4. (a) Time series of measured current height as function of time and distance from the gate, (b) height profile of the current at $t = 6.7$ s, and (c) area of the current as function of time. In (c) the dotted line indicates times where the computed area is not reliable due to difficulty in tracking the current height in the lock at early times.

bulk of the lock fluid has rapidly descended and moved out of the lock. The algorithm can also give erroneous values in regions where the current passes by the five sets of glass guides on the side walls of the tank. These errors are removed and replaced by smoothed values through the application of MATLAB's smoothing function "rlowess."

An example of the measured along-current height versus time is shown in Fig. 8. The time-series plot in Fig. 8(a) clearly shows the advance of an elevated head behind the current nose, with the head height decreasing in time until the current height is monotonically decreasing all the way from tail to nose. It is at this time that the front comes to a near stop at $t = 6.5$ s. The height profile at this time is shown in Fig. 8(b).

At each time for which the height profile is found, we integrate over the entire length of the current to find its area (volume per unit width). In the absence of entrainment this area should be equal, within measurement errors, to the area of the lock fluid, $A_\ell = H_\ell L_\ell$. The corresponding plot of relative current area versus time is shown in Fig. 8(c). The plot is drawn as a dotted line for the first quarter

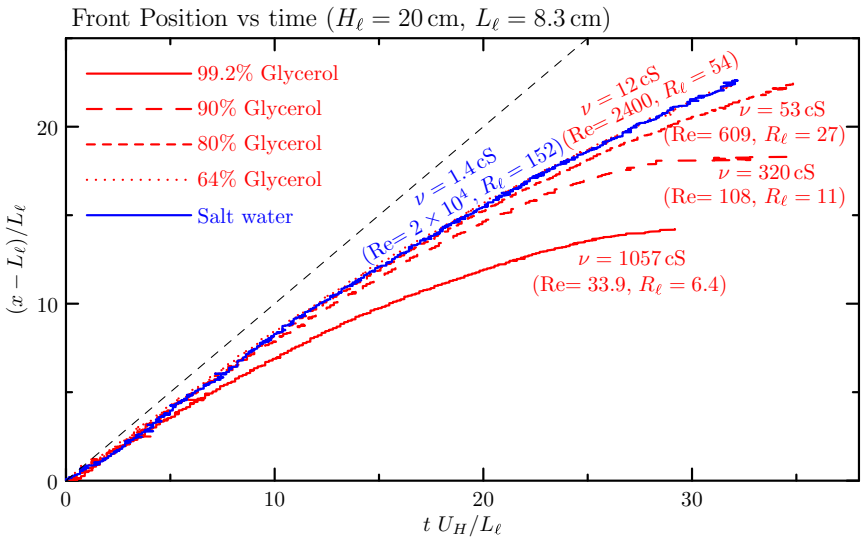


FIG. 9. Front position versus time in experiments with $H_\ell \simeq 20\,\text{cm}$ and $L_\ell = 8.3\,\text{cm}$ and with lock fluids of different densities and viscosities. The horizontal position ahead of the gate is given relative to the lock length, $L_\ell$, and time is given relative to the time for a full-depth lock-release energy-conserving gravity current with speed $U_H$ to travel one lock length. The diagonal dashed black line shows the predicted front position for a current moving at constant speed $U_H$. The meaning of the colored lines are indicated at the upper left of the plot, and the corresponding viscosities and values of Re and $R_\ell$ are indicated toward the right of each curve. Note that the dotted curve, corresponding to 64% glycerol, underlies the blue curve for salt water almost everywhere along its length.

of the time, as a reminder that these values are unreliable due to measurement errors associated with viscous fluid sliding down the side walls of the lock shortly after release of the current. What is clear from this plot is that about 2 s after release the area of the current varies little even as the nose advances and the head height decreases. For times between $1.9 \leqslant t \leqslant 2.1$, the relative area is $1.05 \pm 0.01$ whereas the final relative area is $1.090 \pm 0.005$. This indicates there is relatively little mixing into the current head as it propagates far from the lock.

## IV. QUANTITATIVE RESULTS

Here we present the results of the analyses for a range of experiments of Boussinesq and moderately non-Boussinesq gravity currents moving into fresh water. The experiments reported upon include the classical case of a salt water current as well as currents composed of glycerol with concentrations between 64% and 99.2%. Experiments with full- and partial-depth locks of different lengths are examined.

First we compare how the position of the front versus time depends upon the fluid viscosity in full-depth lock-release experiments. For each of the plots shown in Fig. 9, the corresponding lock height and length of the experiments were fixed at $H_\ell = H = 20(\pm 0.1)\,\text{cm}$ and $L_\ell = 8.3\,\text{cm}$, respectively. Time is normalized in this plot using the predicted energy conserving gravity current speed given by (1).

In the case of a near-saturated salt-water current ($\rho_\ell = 1.14\ \text{g/cm}^3$), the front initially moves at a speed 16% below the predicted speed of an energy conserving gravity current. As is well established, the front slows after moving beyond 6–10 lock lengths as a consequence of transitioning into the self-similar regime [6]. While in this regime the current reaches the end wall of the tank a distance of 23 lock lengths from the gate. That viscosity plays a negligible role over this distance is anticipated

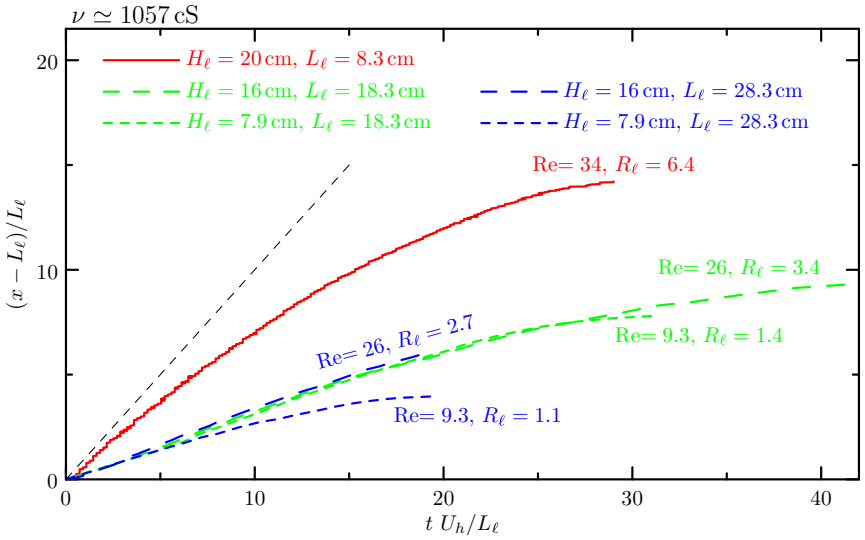


FIG. 10. As in Fig. 9 but showing the front position for experiments with nearly pure glycerol released from locks with different heights and lengths as indicated at the top. In experiments with $H_\ell \simeq 16$ cm, the ambient fluid height is $H = 20$ cm; in experiments with with $H_\ell \simeq 7.9$ cm, the ambient fluid height is $H = 10$ cm. The values of $R_\ell$ are indicated near the end points of each corresponding plot. Time is normalized using the predicted speed, $U_h$, for energy-conserving partial-depth lock-release gravity currents.

from the high Reynolds number (Re $\simeq 1.9 \times 10^4$) and the large ratio of current height to the boundary layer depth given by (10): $R_\ell \simeq 152$.

The front position of a viscous gravity current having a 64% concentration by mass of glycerol, after rescaling time by $L_\ell/U_H$, is found to follow almost the same curve as that of a salt-water current even though its viscosity is 10 times larger. Discrepancies begin to become apparent when the viscosity becomes larger than 0.5 cm$^2$/s (50 cS). In the case of 80% glycerol, the current begins to slow more than the salt water current over the last fifth of the tank. In the cases with 90% ($\nu = 320$ cS) and 99.2% ($\nu = 1057$ cS) glycerol, the current comes to a near stop before reaching the end of the tank. Nonetheless, even in these last two cases the initial relative current speed is close to that of salt water. This is anticipated because $R_\ell \simeq 6$ even for the case of near-pure glycerol. That is, the boundary layer extends over a relatively small fraction of the current after it has propagated a distance of one lock length.

We now turn to examine the evolution of the front position in experiments with near-pure glycerol but with different lock heights and lengths. In all plots of Fig. 10 time is scaled by the current speed, $U_h$, predicted by (3) with $h = H_\ell/2$, which accounts for the speed of energy-conserving partial depth as well as full-depth lock-release currents. Explicitly $U_h = [g' H_\ell(2 - H_\ell/H)]^{1/2}/2$. The case of a full-depth lock release of 99.2% glycerol in a lock of height $H_\ell = 20$ cm and length $L_\ell = 8.3$ cm is reproduced as the solid line in Fig. 10. In this case the initial speed over the first lock length is $(0.79 \pm 0.02)U_h$. In the case of the four partial-depth lock-release experiments for which $H_\ell \simeq 0.8H$, the initial speeds of the currents are found to be $(0.30 \pm 0.02)U_h$, which is significantly smaller than the predicted energy-conserving speed.

A quantitative comparison of the initial speeds in all experiments is shown in Fig. 11, which plots against $R_\ell$ [given by (10)] the ratio of the observed speed to that predicted by (3). These clearly show a sharp drop in the relative speed as $R_\ell$ drops below $\simeq$5.

While the initial speed may not be significantly influenced for currents with $R_\ell$ ranging from 1.1 to 3.1, the near-stopping distance is sensitive to the values of the lock height and length. As a crude estimate of the near-stopping distance, we suppose the current front moves at constant speed $U_h$ until

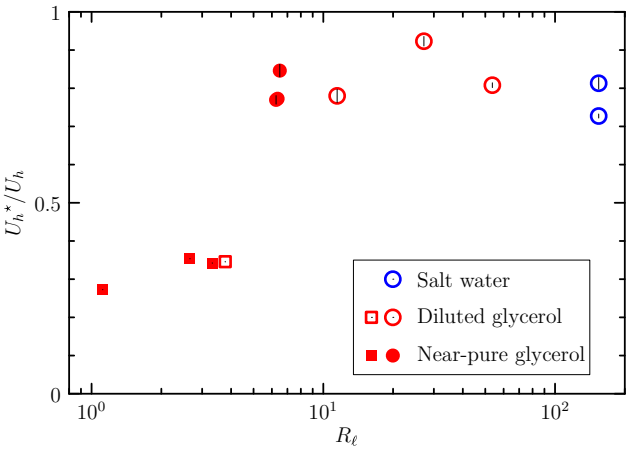


FIG. 11. Measured initial speed of the current front relative to the predicted energy-conserving speed plotted against the current-to-boundary layer height parameter, $R_\ell$. Circles (squares) denote full-depth (partial-depth) lock-release experiments.

coming to a near stop at a distance $X_s$ from the lock end of the tank. Stopping occurs because the boundary layer depth extends over the full depth of the current everywhere along its length. Thus we approximate the height of the current with distance $X_s - x$ behind the front to be proportional to the boundary layer depth such that $h(x,t_s) \propto (\nu(X_s - x)/U_h)^{1/2}$, in which $t_s$ denotes the near-stopping time. Neglecting entrainment into the head, we equate the area under $h(x,t_s)$ to the area of the lock fluid, $A_\ell \equiv H_\ell L_\ell$. Thus we predict that the near-stopping distance is given approximately by

$$X_s \propto \left(U_h {A_\ell}^2/\nu\right)^{1/3}. \tag{11}$$

Figure 12 plots the ratio of the measured near-stopping distance $X_s^\star$ to the right-hand expression of (11). With over a decade of values of $R_\ell$, we find the ratio is approximately constant suggesting

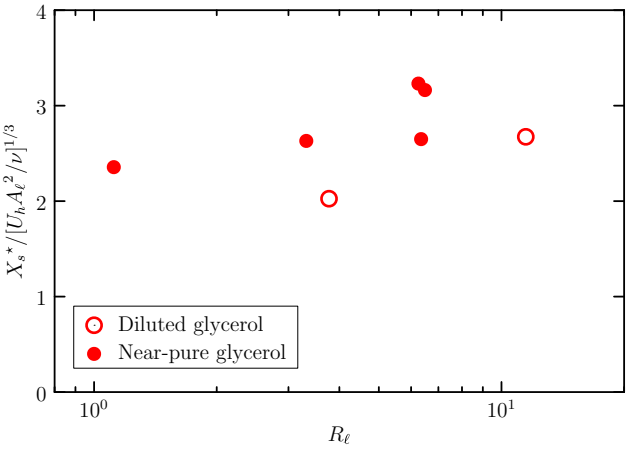


FIG. 12. Measured near-stopping position of the current front relative to the estimated near-stopping scale (11) plotted against $R_\ell$.

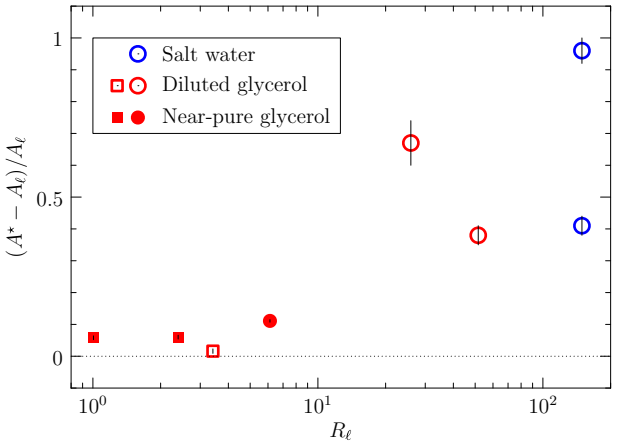


FIG. 13. Net entrainment into current measured through the relative increase in area of the current at the end of an experiment compared with the initial lock area, $A_0 \equiv L_\ell H_\ell$. Circles (squares) denote full-depth (partial-depth) lock-release experiments.

a semiempirical prediction for the near-stopping distance to be

$$X_s = (2.8 \pm 0.4)\big(U_h {A_\ell}^2/\nu\big)^{1/3}. \tag{12}$$

Finally, by determining the height of the gravity current as it evolves over time, we construct an indirect measure of entrainment by finding how the vertical cross-sectional area (volume per unit width) of the current increases compared with the initial area $A_\ell = H_\ell L_\ell$ of fluid in the lock. The area measured when the current comes to a near stop is plotted for different experiments in Fig. 13. For moderately viscous gravity currents with $R_\ell \lesssim 10$, the area increases by less than about 10% of its original area. However, entrainment is substantially larger in experiments with $R_\ell \gtrsim 20$. In those experiments the current propagated to the end of the tank without slowing to a near stop, and the area was computed at the time when the front reached the end of the tank. In a longer tank, the entrainment coefficient is expected to be larger still since the current would continue to entrain while propagating in the self-similar regime.

## V. CONCEPTUAL MODEL

We have found that moderately viscous gravity currents with $R_\ell \lesssim 10$ are not self-similar and that their advance into an ambient fluid of comparable but smaller density is influenced by the return flow into the lock. Such dynamics make it challenging to develop an analytic model describing the flow evolution, not least because of the complicated nature of viscous flow near a corner [16]. Instead, here we develop a conceptual model that attempts to capture the evolution of the gravity current head including only those physical processes suggested by the behavior observed in laboratory experiments. The numerical solution of the resulting model equations is computed in less than 10 s, which is significantly faster than solving the fully nonlinear equations of motion.

### A. Model equations

Our focus is to model the structure and advance of the current head for moderately viscous gravity currents whose initial advance is affected primarily by the return flow and not the viscous boundary layer at the bottom. Rather than model the dynamics of the return flow moving into the lock and impacting the lock end of the tank, we initialize the simulations at a time when the front is already situated approximately one lock length from the gate. This time we denote by $\tau = 0$. Explicitly, as a

model initial condition we set the height of the current along its length to be a power law of the form

$$h(x,\tau=0) = h_0[1-(x/L_0)^2]^p, \tag{13}$$

in which $0 < p < 1$ and the coordinates are set with $x = 0$ at the lock end of the tank. This form, which mimics the structure of a classic viscous gravity current [5] with the choice $p = 1/3$, has the property that $h(0,0) = h_0$, $\partial_x h(0,0) = 0$ and the front becomes vertical asymptotically as $x \to L_0$. The last condition is required because the viscous boundary layer at the front, initially growing with distance behind the nose as $(\nu(L_0 - x)/U_0)^{1/2}$, is likewise vertical at the front. We choose $h_0 = H_\ell/2$, consistent with the theory for energy-conserving partial-depth lock-release gravity currents which predicts that the current height behind the head should be half the lock height. The initial current length, $L_0$, is given by the condition that the area of the current at $\tau = 0$ equals the lock area, $A_\ell$. Explicitly,

$$L_0 = A_\ell\left[h_0\frac{\sqrt{\pi}}{2}\frac{\Gamma(p+1)}{\Gamma(p+1/2)}\right]^{-1}. \tag{14}$$

Assuming the current moves at constant speed $U_0$ from the time of lock release to time $\tau = 0$, we can relate the virtual time $\tau$ to the time $t$ in experiments approximately by $t = \tau + t_0$, in which $t_0 \equiv (L_0 - L_\ell)/U_0$ is the effective start time of the simulations with respect to the time when the fluid is entirely inside the gate.

We assume that the initial boundary layer thickness, $\eta(x,\tau=0)$, is everywhere much smaller than the current height, with the exception of the current front at $x = L_0$, which is a singular point. Explicitly, we take the boundary layer depth to be like that due to an impulsively started infinite plate beneath a viscous fluid:

$$\eta_0(x) \equiv \eta(x,\tau=0) = \begin{cases} 2\sqrt{\nu t_0} = 2\sqrt{\nu(L_0-L_\ell)/U_0}, & 0 \leqslant x \leqslant L_\ell \\ 2\sqrt{\nu(L_0-x)/U_0}, & L_\ell < x \leqslant L_0 \end{cases}. \tag{15}$$

The horizontal flow well above the boundary layer is prescribed so that it smoothly transitions from that of potential flow inside the lock to near-uniform flow outside. Explicitly we set the horizontal flow at $z = h$ to be

$$U_h(x,\tau=0) = U_0\tanh(x/L_\ell), \quad 0 \leqslant x \leqslant L_0. \tag{16}$$

So that it is straightforward to transition between the description of vertical profiles of the flow from circumstances where $\eta \ll h$ to where $\eta \sim h$, we set

$$u(x,z,\tau=0) = \begin{cases} U_h z(2\eta - z)/\eta^2 & 0 \leqslant z \leqslant \eta \\ U_h & \eta < z \leqslant h \end{cases}, \tag{17}$$

in which $h$, $\eta$ and $U_h$ are given by the initial values prescribed, respectively, by (13), (15), and (16). This form of the horizontal velocity field ensures $u = 0$ at $z = 0$ and ensures zero stress at the top of the boundary layer (so that $\partial u/\partial z = 0$ at $z = \eta$). The horizontal velocity is assumed to have the form of (17) at all times such that the time evolution of $u$ is prescribed by changes in $h$, $\eta$, and $U_h$ with the condition $\eta \leqslant h$ for all time. When the boundary layer fills the current depth ($\eta = h$), the $z$ dependence of $u$ is that given by Huppert [5] except that here $U_h$ depends upon its evolution from that given by (16) rather than upon a balance between viscosity and the hydrostatic pressure gradient.

With these prescribed initial conditions, the evolution of the current is set by the condition for mass conservation and the growth of the viscous boundary layer in time. Explicitly the boundary layer depth is advanced in time according to

$$\frac{\partial\eta}{\partial\tau} = \sqrt{\frac{\nu}{t_0+\tau}}. \tag{18}$$

If after this time advancement the resulting boundary layer depth $\eta$ exceeds the current height $h$, then the speed at $z = h$ is adjusted to be $U_h \to U_h h(2\eta - h)/\eta^2$ and $\eta$ is then set equal to $h$. Hence, given the current velocity, the height behind the nose changes in time according to

$$\frac{\partial h}{\partial \tau} = -\frac{\partial \mathcal{F}}{\partial x} \tag{19}$$

in which the volume flux per width, $\mathcal{F}$, is given by the integral

$$\mathcal{F} \equiv \int_0^h u\, dz = U_h(h - \eta/3). \tag{20}$$

This equals $2U_h h/3$ where the boundary layer has grown to the height of the current. The current front is assumed to advance at speed $U_h(x = \mathrm{x_N}, \tau)$ until all the fluid in the current head is consumed in the boundary layer.

Because the stress of the ambient flow upon the viscous current is negligible, the return flow passing over the current plays no role in the evolution of the current other than setting its initial maximum flow speed, $U_0$, as a consequence of pressure gradients set up by the speed of the return flow passing over the current. The speed of the return flow is set by the condition for mass conservation assuming a rigid, free-slip surface condition: $u_r(x,z,\tau) = -\mathcal{F}/(H - h)$ for $h < z \leqslant H$ and $x < \mathrm{x_N}$. The ambient flow is assumed to be zero for $x > \mathrm{x_N}$.

### B. Numerical implementation

The equations above are discretized on a staggered finite-difference grid. The current height, $h$, and boundary layer height, $\eta$, are represented by $N + 1$ equally spaced points in the horizontal on the "regular grid" from $x = 0$ to $x = \mathrm{x_N}$, corresponding to a horizontal resolution of $\Delta = \mathrm{x_N}/N$. The current speed, $U_h$, and volume flux per width, $\mathcal{F}$, are represented on the "staggered grid" by $N$ equally spaced points ranging between $\Delta/2$ to $\mathrm{x_N} - \Delta/2$.

The average of the neighboring values of $h$ and $\eta$ are used in (20) to compute $\mathcal{F}$. Neighboring differences of $\mathcal{F}$ are then used to compute $\partial h/\partial t$ on the regular grid for $\Delta \leqslant x \leqslant \mathrm{x_N} - \Delta$. Under the assumption of no horizontal flow at $x = 0$, the change in height at $x = 0$ is taken to be $-\mathcal{F}|_{x=\Delta/2}/(\Delta/2)$. With the assumption that the current front advances in a small time $\Delta_\tau$ to $\mathrm{x_N} + \Delta_N$ with $\Delta_N = U_h \Delta_\tau$, the change in height at $x = \mathrm{x_N}$ is set by volume conservation so that

$$\left.\frac{\partial h}{\partial \tau}\right|_{\mathrm{x_N},\tau} = \frac{1}{\Delta_\tau}\left[(1/8)\Delta h|_{\mathrm{x_N}-\Delta,\tau} + \mathcal{F}|_{\mathrm{x_N}-\Delta/2,\tau}\Delta_\tau\right]\Big/(\Delta_N + \Delta/2). \tag{21}$$

Given $\partial h/\partial \tau$, $h$ is advanced to time $\tau + \Delta_\tau$ on the regular grid. The grid is then rescaled to extend from $x = 0$ to $\mathrm{x_N}|_{\tau+\Delta_\tau}$ by $N + 1$ points, and linear interpolation is used to represent $h$ on this new grid specifying $h = 0$ at $\mathrm{x_N}|_{\tau+\Delta_\tau}$. Likewise, the boundary layer depth is interpolated onto this new grid. The velocity field may then be defined on the rescaled staggered grid according to (17) and (16) using the updated values of $h$ and $\eta$. Likewise the volume flux is computed on the rescaled staggered grid. As a diagnostic, the ambient flow above the current on the rescaled staggered grid is $-\mathcal{F}/(H - h)$.

The code iterates through this procedure, computing the change in time to $h$ and $\eta$, advancing these fields with an area-conserving nose condition, recomputing $h$, $\eta$ by interpolation onto the rescaled regular grid and then recomputing $\mathcal{F}$ on the rescaled staggered grid.

### C. Results

Figure 14 shows snapshots from a simulation initialized with the parameters of the experiment shown in Fig. 4. As with this experiment, the model is initialized with a gravity current having viscosity $\nu_\ell = 11$ cm$^2$/s and density $\rho_\ell = 1.26$ g/cm$^3$ originating from a full-depth lock of height $H_\ell = H = 20$ cm and length $L_\ell = 8.3$ cm. The current propagates into water of viscosity 0.01 cm$^2$/s and density 0.998 g/cm$^3$. The simulation starts at the effective time $t_0 = 0.335$ s. The initial current

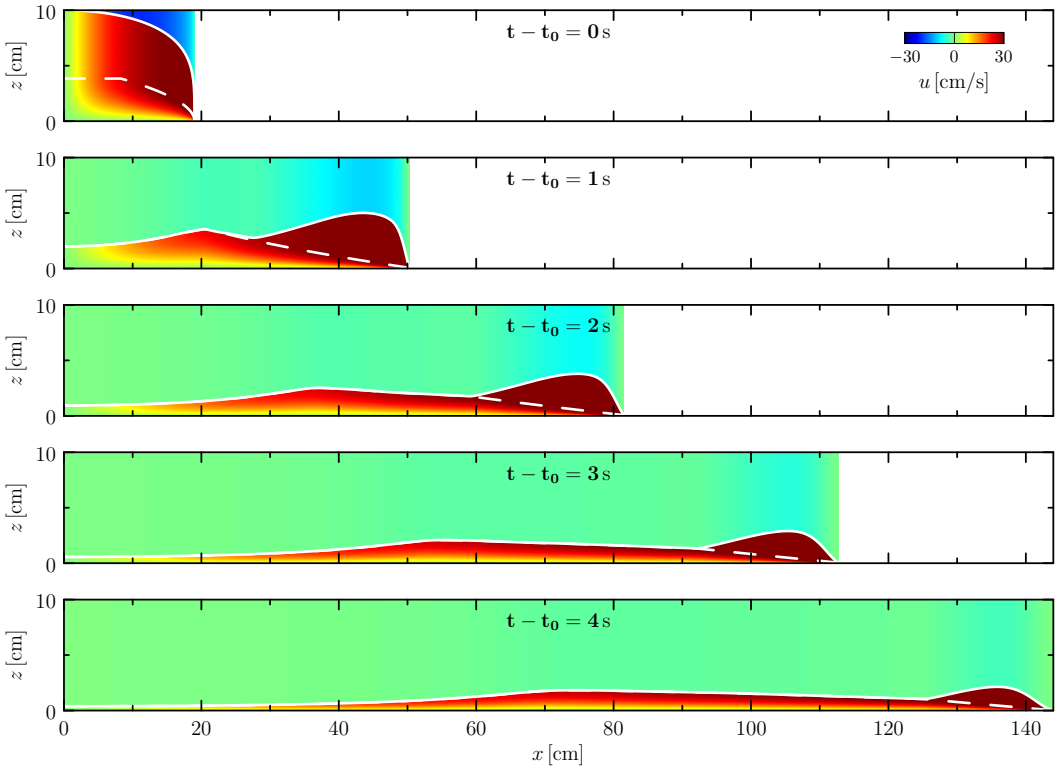


FIG. 14. Horizontal velocity of current and return flow computed from the conceptual model with initial conditions determined from those of the experiment shown in Fig. 4. In each plot, the height of the current is indicated by the solid white line and the white dashed lines indicate the height of the viscous boundary layer. Only half the vertical extent of the domain is shown. The color scale for horizontal speed in all plots is given in the upper-right corner of (a). Color is plotted only between the lock end of the tank and the current nose. Beyond, the ambient fluid is assumed to be stationary and not included in the model.

height is given by (13) with $h_0 = H_\ell/2$ and $p = 1/4$. The corresponding initial length of the current is $L_0 = 19.0\,\mathrm{cm}$.

While the flow near the lock end of the tank shallows faster than observed, the simulation does reproduce the formation of an elevated head that advances rightward decreasing in maximum height until the current comes to a near stop after $\tau = 4.2\,\mathrm{s}$ ($t \simeq 4.5\,\mathrm{s}$) at $\mathrm{x_N} = 150\,\mathrm{cm}$. Despite the crude approximations of the model, the simulated near-stopping time and distance are comparable to those observed in the experiment.

## VI. DISCUSSION AND CONCLUSIONS

Laboratory experiments show that a viscous gravity current of glycerol flowing into water evolves qualitatively differently from that of a viscous gravity current flowing into air. While the latter adopts the monotonic self-similar shape predicted by (7) and its nose advances as a one-fifth power of time, a viscous gravity current in water has a nonmonotonic shape with a head that is elevated above the trailing current and whose nose advances at near-constant speed until the head flattens out and the current comes to a near stop.

The explanation for this evolution, supported by a conceptual model, is that the return flow into the lock sets up an adverse pressure gradient that retards the advance of the current. This builds up a current head whose depth is significantly larger than the boundary layer depth behind the nose.

Because the viscous stresses are negligible over the top of the head, the fluid in the current above the boundary layer is free to advance without the influence of viscous forces to slow it down. Like an unfurling carpet, this fluid moves toward the nose where it comes into contact with tank bottom, thereafter lying within the viscous boundary layer behind the nose. In this way the freely flowing fluid in the head above the boundary layer becomes lost to the boundary layer. Correspondingly the head height decreases until it flattens out at which time the viscous boundary layer extends over the depth of the current along its whole length. Being formed in this way, the current has an approximate wedge shape when the head flattens: there is no steep rise of the current height immediately behind the nose as is the case for self-similar viscous gravity currents. Thus near the nose viscous forces dominate over buoyancy forces manifest through horizontal pressure gradients establish by hydrostatic balance. It is for this reason that the current comes to a near stop.

These proposed dynamics inspired classification of the importance of viscosity upon the initial current speed in terms of the ratio $R_\ell$ of the initial current depth to the characteristic boundary layer depth, which itself is related to the Reynolds number and the aspect ratio of the fluid in the lock. The speed was found to slow substantially if $R_\ell \lesssim 5$. Likewise, the proposed dynamics were used to formulate a semiempirical prediction (12) for the distance at which the current comes to a near stop. Entrainment into the current was estimated by comparing the volume per width of the current when it comes to a near stop (or reaches the end of the tank) to the volume per width of fluid initially in the lock. Entrainment was found to be relatively small if $R_\ell \lesssim 7$, in which case the area increased by less than 10%. In comparison, the increase was between 40% and 100% if $R_\ell \gtrsim 20$.

This idealized study demonstrates that the theory of Huppert [5] in the specific case of lock-release viscous gravity currents well predicts their evolution only if their density is much larger than the ambient fluid into which it propagates so that the ambient fluid always plays a passive role from initial release to consequent evolution. If the ambient fluid has comparable density to the lock fluid, then the return flow into the lock non-negligibly influences the structure and speed of the current at early times and consequently changes the evolution of the current at moderate times thereafter.

## ACKNOWLEDGMENTS

Inspiration for this work arose from conversations with Rama Govindarajan during the KITP "Follow-on" meeting organized by Eckart Meiburg at UC Santa Barbara in April 2014. This research was supported in part by funding for Y.S.H. through the University of Toronto's Engineering Science Research Opportunities Program (ESROP) and by funding through the Discovery Grant program of the Natural Sciences and Engineering Research Council of Canada (NSERC).

[1] J. E. Simpson, *Gravity Currents*, 2nd ed. (Cambridge University Press, Cambridge, 1997), p. 244.
[2] H. E. Huppert, Gravity currents: A personal perspective, J. Fluid Mech. **554**, 299 (2006).
[3] T. B. Benjamin, Gravity currents and related phenomena, J. Fluid Mech. **31**, 209 (1968).
[4] N. Didden and T. Maxworthy, The viscous spreading of plane and axisymmetric gravity currents, J. Fluid Mech. **121**, 27 (1982).
[5] H. E. Huppert, The propagation of two-dimensional and axisymmetric viscous gravity currents over a rigid horizontal surface, J. Fluid Mech. **121**, 43 (1982).
[6] J. W. Rottman and J. E. Simpson, Gravity currents produced by instantaneous releases of a heavy fluid in a rectangular channel, J. Fluid Mech. **135**, 95 (1983).
[7] T. von Kármán, The engineer grapples with nonlinear problems, Bull. Am. Math. Soc. **46**, 615 (1940).
[8] J. W. Rottman and P. F. Linden, Gravity currents, in *Environmental Stratified Flows*, edited by R. Grimshaw (Kluwer Academic Publishers, Dordrecht, 2002), pp. 89–118.
[9] R. J. Lowe, J. W. Rottman, and P. F. Linden, The non-Boussinesq lock-exchange problem. Part 1. Theory and experiments, J. Fluid Mech. **537**, 101 (2005).

[10] J. O. Shin, S. B. Dalziel, and P. F. Linden, Gravity currents produced by lock exchange, J. Fluid Mech. **521**, 1 (2004).
[11] H. E. Huppert and J. E. Simpson, The slumping of gravity currents, J. Fluid Mech. **99**, 785 (1980).
[12] Z. Borden and E. Meiburg, Circulation based models for Boussinesq gravity currents, Phys. Fluids **25**, 101301 (2013).
[13] T. Bonometti and S. Balachandar, Effect of Schmidt number on the structure and propagation of density currents, Theor. Comput. Fluid Dyn. **22**, 341 (2008).
[14] R. C. Weast, *Handbook of Chemistry and Physics*, 62nd ed. (CRC Press, Boca Raton, FL, 1981).
[15] C. Härtel, E. Meiburg, and F. Necker, Analysis and direct numerical simulation of the flow at a gravity-current head. Part 1. Flow topology and front speed for slip and no-slip boundaries, J. Fluid Mech. **418**, 189 (2000).
[16] H. K. Moffatt, Viscous and resistive eddies near a sharp corner, J. Fluid Mech. **18**, 1 (1964).
[17] See Supplemental Material at http://link.aps.org/supplemental/10.1103/PhysRevFluids.3.034101 for movies of the experiments with snapshots shown in Figs. 2, 4, and 7.